DESIGN AND CHARACTERIZATION OF MEMS VARACTOR

Suma N*[1], S.L.Pinjare*[2]

Dept. of Electronics & Communication Engineering,

Nitte MIT, Bangalore

E-mail: [1]suma.nagappa@gmail.com,)

Abstract—**The greatest promise of MEMS (microelectromechanical systems) lies in the ability to produce mechanical motion on a small scale. Such devices are typically low power and fast, taking advantage of such micro-scale phenomena as strong electrostatic forces and rapid thermal responses. The variable capacitor is designed by first designing the bi-directional vertical actuator which can produce both upward and downward motion. We find the temperature distribution of the hot and the cold arm of the actuator and the maximum deflection because of the applied voltage. Finally a variable capacitor is designed with the vertical actuator. The capacitor tuning range was found to be from 2.2 pF to 0.044 pF. The variable capacitor has been designed in the PolyMUMS fabrication process. Compared to electrostatic, tuneable capacitors actuated by thermal actuators have several advantages such as no pull in effect, low driving voltages etc. The design and simulation of the MEMS thermal actuator and variable capacitor is done by using Coventorware 2010 and Comsol 4.1.The numerical result is generated by using MemETherm solver.**

Keywords- MEMS, Thermal actuator, **tuneable capacitors**

I. INTRODUCTION

It can be said that the field of microelectromechanical systems (MEMS) was originated by Richard P. Feynman in 1959, when he made the observation: “There’s plenty of room at the bottom” [1].He was the first one to induce the idea of ***miniaturization of systems.*** MEMS can also be defined as (MEMS) is the integration of mechanical elements, sensors, actuators, and electronics on a common silicon substrate through micro fabrication technology. While the functional elements of MEMS are miniaturized structures, sensors, actuators, and microelectronics, the most notable (and perhaps most interesting) elements are the microsensors and microactuators. Microsensors and microactuators are appropriately categorized as “transducers”, which are defined as devices that convert energy from one form to another. In the case of microsensors, the device typically converts a measured mechanical signal into an electrical signal. The electronics can be fabricated by IC process sequence (e.g., CMOS) and the mechanical elements are constructed by micromachining methods that are compatible with the IC fabrication process. MEMS promises to revolutionize nearly every product category by bringing together silicon-based microelectronics with micromachining technology, making possible the realization of complete **systems-on-a-chip**.

There are different types of actuators such as electro-static actuator in which the electrostatic force is created by applying the voltage across the two plates. But in order to have a large deflection or force, high actuating voltage is needed. Also, hysteresis makes the electrostatic microactuator hard to control. Hence we use the next type of actuator namely the thermal actuator. Thermal actuator has several advantages such as Avoiding the static charges collecting on the plates, Improvement in the reliability, Lower driving voltages and mainly no pull in effect.. These thermal actuators are used in micro legs, micro grippers, micro positioning applications etc. In the sections 2 we design a vertical actuator and do the electro thermal analysis and mechanical analysis of the actuator using COMSOL. In section 3 we design the variable capacitor using the vertical actuator.

II. VERTICAL ACTUATOR

A. Vertical Thermal Actuator

Vertical thermal actuator is the one that can have the motion perpendicular to the substrate. This vertical thermal actuator (VTA) can either bend upward or downward. The bending direction of the new VTA depends on where the voltage is applied. When the voltage is applied across anchors 1 and 2 in Figure 1, the current only goes through the top layer, and it expands due to the increase of its temperature. Thus, the actuator’s tip is deflected downward to the substrate. For deflecting the actuator upward, the voltage is simply switched from anchors 1 and 2 to anchors 3 and 4. The U-shape VTA is more electrically efficient than the traditional actuator since no electrical power is wasted in the cold arm when the U-shape vertical actuator is operated. This bidirectional motion indicates that the new vertical thermal actuator has almost twice amount of displacement compared to the conventional VTA at the same size. The current only goes through the top layer, and it expands due to the increase of its temperature.

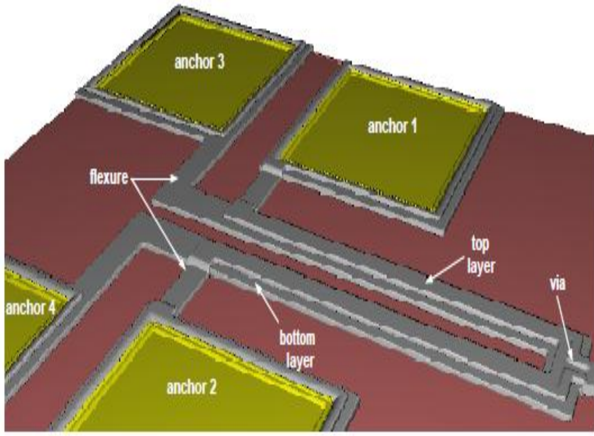

Figure 1: A schematic top view of the U-shape VTA

B. Modeling and Analysis

A schematic top view diagram of the U-shape VTA is shown in Figure 1. Since the U-shape VTA is fabricated by using surface micromachining, the electro-thermal analysis of the U-shape VTA can be simplified as one dimensional heat transfer problem similar to the thermal analysis of the two-hot arm thermal actuator. When the U-shape VTA is operated, the current only passes through one layer of the actuator. In the following analysis, the current is assumed to pass through the top layer of the actuator.

The actuator shown in Figure 1 can be seen as several microbeams connected in series. The coordinate system for the thermal analysis is shown in Figure 3. In this coordinate system, there are five microbeams connected to each other.

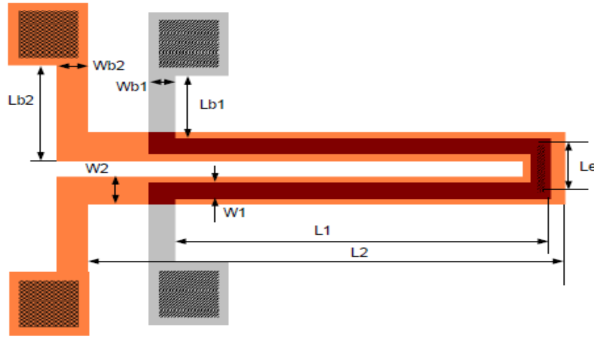

Figure 2 :2-D VTA

The two short and long bars of the microbeams have the same dimensions. In order to simply the analysis, the two short bars are numbered as element 1, the two long beams are named as element 2, and the connection between two long beams is shown as element 3. The thermal analysis of the U-shape VTA is similar to the thermal analysis of the two-hot arm thermal actuator. Only the heat loss through conduction and convection is concerned, and the heat that is dissipated through radiation to the ambient is neglected based on the previous finite element analysis. Under steady-state conditions, ohmic power generated in the element is equal to heat conduction and convection out of the element,

$$-K_P wt[\frac{dT}{dx}]_x + J^2\rho wt dx = -K_P wt[\frac{dT}{dx}]_{x+dx} + \frac{Sw(T-T_s)dx}{R_T} \quad (1)$$

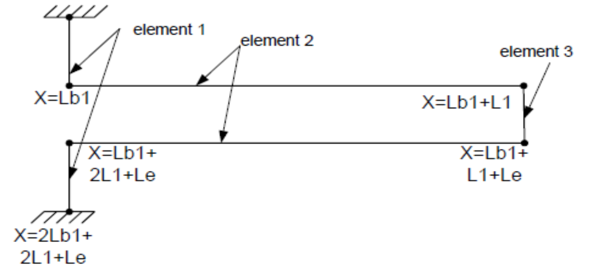

Figure3: Simplified one dimensional coordinate system

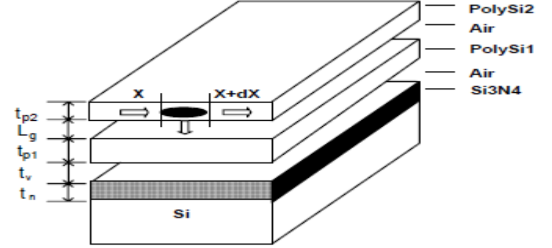

Figure3: Schematic cross section for thermal analysis

The general solution to the temperature distribution of each element of the U-shape VTA can be written as:

$$T = T_s + \frac{B}{A^2} + C_1 e^{Ax} + C_2 e^{-Ax}$$

where C_i (i = 1 to 6) are the constants to be obtained. For simplification, A and B are employed to represent two long terms during solving Equation 1. The subscript is assigned to them for different elements in the following. For element 1, the temperature distribution is

$$T_1 = T_s + \frac{B_1}{A_1^2} + C_1 e^{Ax} + C_2 e^{-A_1 x} \quad (2)$$

where

$$A_1^2 = \frac{S_{b1}}{k_p R_{T1} t_{p2}} + B_1 \xi$$

$$B_1 = \frac{V_{b1}^2}{L_{b1}^2 \rho_0 k_p}$$

$$V_{b1} = \frac{V}{2(L_{b1}+L_1)+L_e} L_{b1}$$

$$S_{b1} = \frac{t_{p^2}}{w_{b1}}\left[\frac{2(L_g+t_{p1}+t_v)}{t_{p^2}}+1\right]+1$$

$$R_{T1} = \frac{t_v+L_g}{k_v}+\frac{t_n}{k_n}+\frac{t_{p1}}{k_p}$$

and V_{b1} is the potential acted on element 1; S_{b1} is the shape factor of element 1. For element 2, the temperature distribution is similar to element 1 except that L_{b1} is replaced byL_1, and w_{b1} is replaced by w_1, that is

$$T_2 = T_s + \frac{B_2}{A_2^2} + C_3 e^{A_2 x} + C_4 e^{-A_2 x} \quad (3)$$

where

$$B_2 = \frac{V_{b2}^2}{L_1^2 \rho_0 k_p}$$

$$S_{b2} = \frac{t_{p^2}}{w_1}\left[\frac{2(L_g+t_{p1}+t_v)}{t_{p^2}}+1\right]+1$$

$$V_{b2} = \frac{V}{2(L_{b1}+L_1)+L_e} L_1$$

$$A_1^2 = \frac{S_1}{k_p R_{T1} t_{p^2}} + B_2 \xi$$

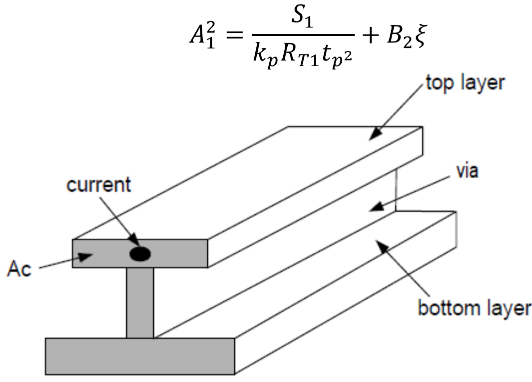

Figure 4: 3D schematic diagram of the element 3

Element 3 is the connection between the top layer and the bottom layer, the cross section of element 3 is not rectangular like elements 1 and 2. Figure 4 shows the 3-D view of the cross section of element 3. For element 3, under steady state, the heat flow Equation 1 takes the form

$$k_p A_v \frac{d^2T}{dx^2} = \frac{S_e w_2 (T - T_{S)}}{R_{T2}} - J^{2\rho A_c} \qquad (4)$$

where A_v is the sum of the cross sections of the top layer, via, and bottom layer of the element 3, A_c is the cross section of the top layer in element 3, and S_e is the shape factor for element 3. Solving the above Equation the temperature distribution of element 3 can be obtained as

$$T_3 = T_s + \frac{B_3}{A_3^2} + C_5 e^{A_3 x} + C_6 e^{-A_3 x} \qquad (5)$$

where

$$B_3 = \frac{V_{b3}^2 A_e}{L_e^2 \rho_0 k_p A_v}$$

$$V_{b3} = \frac{V}{2(L_{b1} + L_1) + L_e} L_e$$

$$A_3^2 = \frac{S_e w_2}{k_p R_{T2} A_v} + B_3 \xi$$

$$S_e = \frac{t_{p1}}{w_2}\left[\frac{2t_v}{t_{p1}} + 1\right] + 1$$

$$R_{T2} = \frac{t_v}{k_v} + \frac{t_n}{k_n}$$

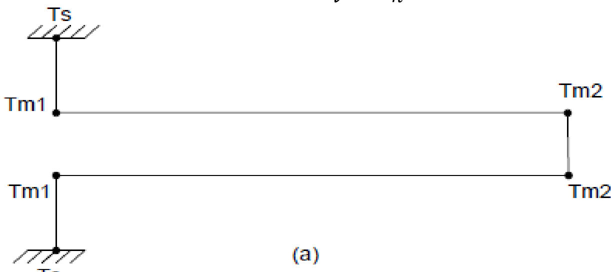

Figure 5 (a): The boundary conditions of temperature continuity.

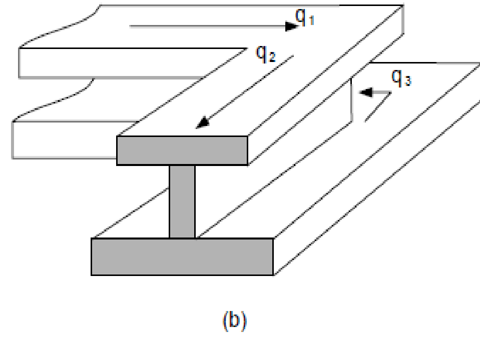

Figure 5(b): The boundary conditions of the rate of the heat conduction

In order to solve for constants C_i (i = 1 to 6) in Equations (2), (3), and (5), at least six boundary conditions are needed. Figure 5 (a) shows the boundary conditions that represent the continuity of temperature from one element to another. Since the U-shape VTA is symmetrical, the temperature distribution of the actuator also should be symmetrical. Therefore, the temperatures of both ends of element 3 are equal to Tm2, and the two joints between elements 1 and 2 are equal to Tm1. Figure 5 (b) shows the boundary conditions of the rate of the heat flow. Substituting all the boundary conditions into Equations (2), (3) and (5), the following equations are obtained where

$$\overline{AC} = \bar{B} \qquad (6)$$

$$\bar{A} = \begin{pmatrix} 1 & 1 & 0 & 0 & 0 & 0 & 0 & 0 \\ e^{A1L_{b1}} & e^{-A1L_{b1}} & 0 & 0 & 0 & 0 & 0 & 0 \\ 0 & 0 & 1 & 1 & 0 & 0 & -1 & 0 \\ 0 & 0 & e^{A3L_1} & e^{-A3L_1} & 0 & 0 & 0 & -1 \\ 0 & 0 & 0 & 0 & 1 & 1 & 0 & -1 \\ 0 & 0 & 0 & 0 & e^{A3L_e} & e^{-A3L_e} & 0 & -1 \\ A_1 e^{A1L_{b1}} & -A_1 e^{-A1L_{b1}} & -A_2 & A_2 & 0 & 0 & 0 & 0 \\ 0 & 0 & \lambda e^{A_3 L_1} & -\lambda e^{-A_3 L_1} & e^{A3L_1} & -e^{-A3L_1} & 0 & \frac{-R}{h_p w_2 t_{p1} A_3} \end{pmatrix}$$

$$\bar{B} = \begin{pmatrix} -\frac{B_1}{A_1} \\ -T_S - \frac{B_1}{A_1^2} \\ -T_S - \frac{B_1}{A_1^2} \\ -T_S - \frac{B_1}{A_1^2} \\ -T_S - \frac{B_1}{A_1^2} \\ -T_S - \frac{B_1}{A_1^2} \\ 0 \\ \frac{-RT_S}{k_p w_2 t_{p1}} \end{pmatrix} \qquad \bar{c} = \begin{pmatrix} C_1 \\ C_2 \\ C_3 \\ C_4 \\ C_5 \\ C_E \\ T_{m1} \\ T_{m2} \end{pmatrix}$$

Here λ is equal to $\frac{w_1 t_{p2} A_2}{w_2 t_{p1} A_3}$, R is the thermal resistance of the bottom layer of the U-shape vertical thermal actuator, and it is calculated by

$$R = \frac{K \frac{A_1}{L_1} \frac{A_2}{L_{b1}}}{\frac{A_1}{L_1} + \frac{A_2}{L_{b1}}}$$

where A_1 and A_2 are the cross section area of the long bar and short bar, respectively. Solving Equation (6) and substituting

the given process parameters to Equations (2), (3) and (5), the temperature distribution of the U-shape VTA can be obtained

C .Simulation results

Figure 6 shows the temperature distribution of the U-shaped vertical thermal actuator. The input voltage is 5V, and the other parameters are listed in Tables 1 and 2. Since the U-shaped vertical thermal actuator is symmetrical about its center line, the temperature distribution also should be symmetrical about its center line. The above analytical results show that characteristic. The maximum temperature appears in element 2 rather than element 3. This is because element 3 is the connection between the top and bottom layers. The bottom layer becomes a heat sink which reduces element 3 temperature. Also, the cross section of element 3 is bigger than that of element 2, hence element 3 has a bigger thermal capacitance compared to element 2.

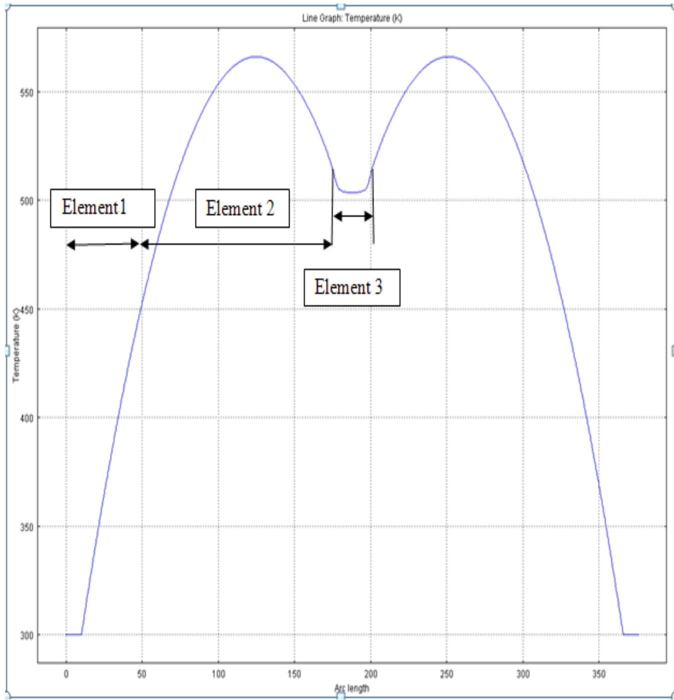

Figure 6: Temperature distribution along the top layer

Material Properties	Value	Unit
Young's modulus E	162×10^{9}	Pa
Poisson's ratio $\boldsymbol{v}$	0.22	
Thermal expansion coefficient K	4.7×10^{-6}	C^{-1}
Thermal conductivity of polysilicon k_p	41×10^{-6}	w.$\mu m^{-1}.C^{-1}$
Thermal conductivity of air k_v	0.026×10^{-6}	w.$\mu m^{-1}.C^{-1}$
Thermal conductivity of nitride k_n	2.25×10^{-6}	w.$\mu m^{-1}.C^{-1}$
Resistivity of polysilicon ρ_0	20	Ω. µm
Linear temperature Coefficient ξ	1.25×10^{-3}	C^{-1}

Table 1: Material properties

Geometrical data	Value	Unit
The length of the long beam of the top layer L1	177	µm
The length of the long beam of the bottom layer L2	217	µm
The length of the short bar of the top layer Lb1	50	µm
The length of the short bar of the bottom layer Lb2	60	µm
The width of the long beam of the top layer w1	10	µm
The width of the long beam of the bottom layer w2	18	µm
The width of the short bar of the top layer wb1	13	µm
The width of the short bar of the bottom layer wb2	15	µm
The length of the connection between two long beams Le	38	µm
The gap between the top layer and the bottom layer	0.75	µm
The thickness of the top layer Tp2	1.5	µm
The thickness of the bottom layer Tp1	2.0	µm
The thickness of air Tv	2	µm
The thickness of nitride Tn	0.6	µm

Table 2: Geometrical data of the U-shaped vertical thermal actuator

Figure 6 shows the numerical simulation of the same actuator using Coventorware software. In this simulation, three different physical domain boundary conditions, electrical, thermal and mechanical, are applied. In the electrical boundary condition, the actuating voltage is added across anchors 1 and 2 in Figure 1. All of the four anchors are set to the substrate temperature for the thermal boundary condition since they are connected to the substrate. For the mechanical boundary conditions, these four anchors are also fixed in all directions. The simulation results are shown in Figure 7. The temperature distribution is in good agreement with the analytical results. The maximum temperature as a function of the input voltage is also provided in Figure 8 Like the two-hot arm thermal actuator and for the same reason, the analytical results are in better agreement with the numerical results at low voltage. However, the difference at high input voltages is acceptable.

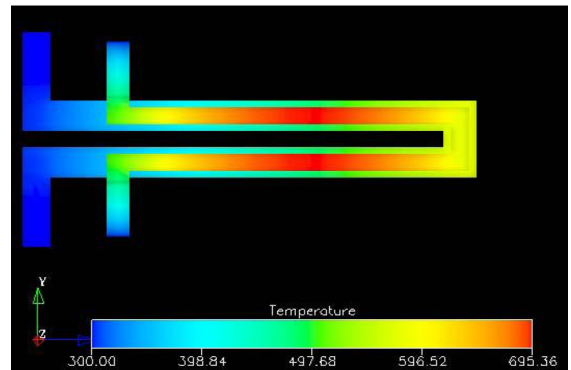

Figure 7: Temperature distribution

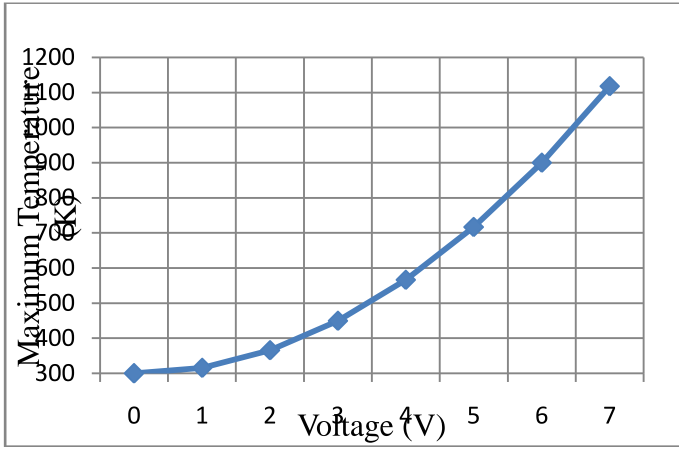

Figure 8:Maximum temperature at different voltage

The below figures, figure 9 and figure 10 gives the Comsol results with the voltage is applied to anchor 1 and 2 and then to anchor 3 and 4 respectively

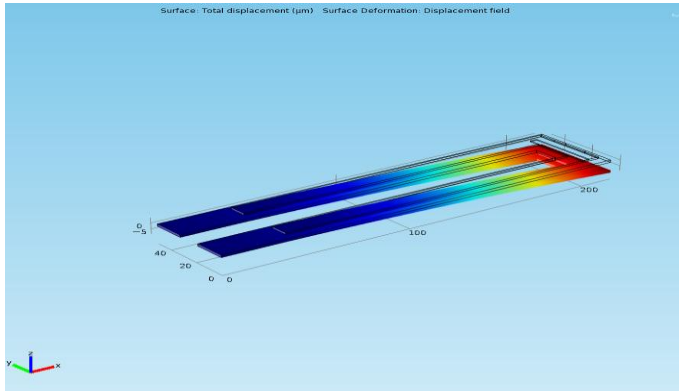

Figure 9: Deflection downwards

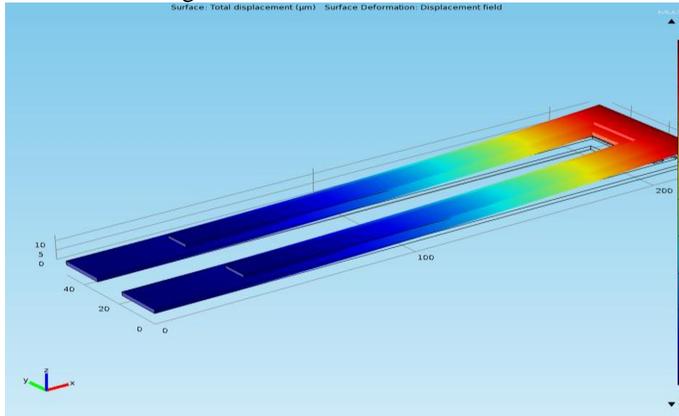

Figure 10: Deflection upwards

D Mechanical analysis: Analytical solution

The linear thermal expansions of the top and bottom layers are the essential inputs for the mechanical analysis of the U-shape vertical thermal actuator. Based on Equation (3), the thermal expansion of the top layer can be obtained from

$$\Delta L_1 = \propto \int_0^{L_1} (T - T_s)dx = \propto \left[\frac{B_2}{A_2^2} L_1 + \frac{C_3}{A_2}\left(e^{A_2 L_1} - 1\right) - \frac{C_4}{A_2}\left(e^{-A_2 L_1} - 1\right)\right]$$

where the parameters.Here, the thermal expansions of elements 1 and 3 of the top layer are neglected in comparison with the thermal expansion of element 2. From Figure 7, it is clear that the temperature of the bottom layer is also increased. Since, no current passes through the bottom layer, the temperature distribution along the bottom layer is a simple linear heat conduction problem. The thermal expansion of the bottom layer can be calculated by

$$\Delta L_2 = \propto \int_0^{L_2} (T - T_s)dx = \frac{1}{2} \propto (T_{m2} - T_s)L_2$$

where Tm2 is the tip temperature of the bottom layer as shown in Figure 7.7 (a).

Since the U-shape VTA is symmetrical, it can be simplified to that shown in Figure 5(a).In this section, it is intended to convert the continuous model shown in Figure11(a).to a lumped model four-bar linkage shown in Figure 11(b).In this model, element 1 (short bar) is treated as a torsional spring, because when the tip of the U-shape vertical thermal actuator is bent upward or downward, element 2 (long beam) rotates about element 1 (short bar).

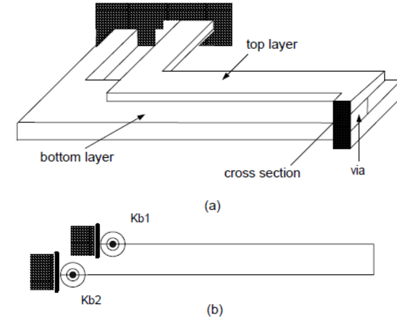

Figure 11: (a) The schematic 3-D view

(b) Four bar linkage representingU-shaped VTA.

The deflection of the VTA can be calculated by the following steps. First, the deflection of the structure shown in Figure 12 (a) After that, the spring coefficient K_T of the structure in the y direction at the tip of the actuator can be found (Figure 12 (b)). Then, the whole structure in Figure 7.14 (b) can be redrawn as the one in Figure 12.Here, the base of the plane rigid frame shown in Figure 12 (b) is hinged and therefore two force components can be used when the hinged base is released (12 (a)). The two force components (X_1 andX_2) can be calculated by solving Equation (7):

$$\begin{bmatrix} f_{11} & f_{13} \\ f_{21} & f_{22} \end{bmatrix} \begin{bmatrix} X_1 \\ X_2 \end{bmatrix} = \begin{bmatrix} \Delta L_1 - \Delta L_2 \\ 0 \end{bmatrix} \qquad (7)$$

where fij represents the flexibility coefficients, and they all can be obtained by

$$f_{11} = \frac{L_2^3}{3EI_2} + \frac{L_2^2 L_g}{EI_g} + \frac{L_2^2 L_1}{EI_1} - \frac{L_1^3}{3EI_1}$$

$$f_{21} = \frac{L_1^2 L_g}{2EI_1} - \frac{L_2 L_g L_1}{EI_1} - \frac{2L_g^2 L_2}{3EI_g}$$
$$f_{12} = f_{21}$$
$$f_{22} = \frac{L_g^3}{3EI_g} + \frac{L_g^2 L_1}{EI_1}$$

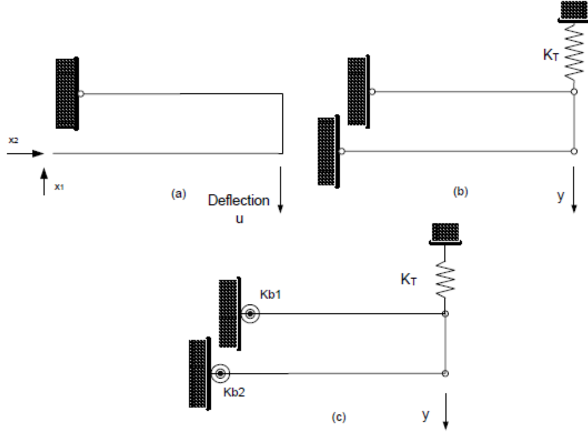

Figure 12: (a) The hinged rigid frame for mechanical analysis,

(b) Schematic of the spring coefficient analysis in y direction.

(c) Schematic of the deflection of the U-shape VTA.

Once the two force components are achieved, the deflection of the end of the rigid frame without torsional spring (Figure 12(a)) can still be calculated by using the virtual work method. The bending moment of the top layer long beam due to the virtual force is shown in Figure 13 (a).

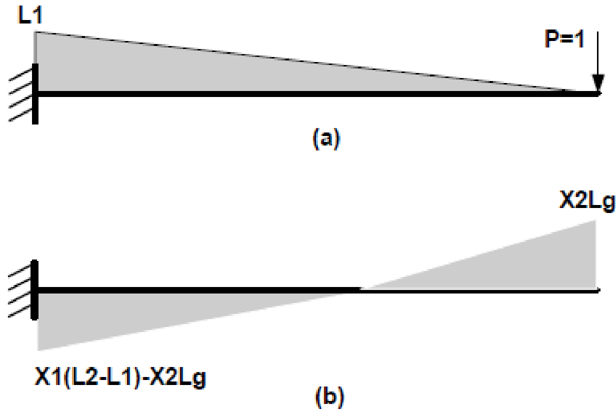

Figure 13: (a) The bending moment of the top layer long beam due to the virtual force,

(b) The bending moment of the top layer long beam due to the thermal expansion.

The bending moment due to the virtual force as a function of the position of the top layer long beam is given by

$$\bar{M} = L_1 - x$$

The bending moment due to the thermal expansion is shown in Figure 13 (b). It can be obtained by

$$M = X_1 x + X_1(L_2 - L_1) - X_2 L_g$$

According to the virtual work method, the deflection of the hinged rigid frame without the
torsional springs (Figure 12 (a)) can be found as

$$u = \frac{1}{EI_1}\int_0^{L_1} M\bar{M}dx = \frac{1}{EI_1}(-\frac{1}{3}X_1 L_1^3 + \frac{1}{2}X_1 L_1^3 L_2 - \frac{1}{2}X_2 L_1^2 L_g$$

In order to find the stiffness coefficient KT in Figure 11 (b), three deflections are assigned to the hinged rigid frame structure (Figure 13)

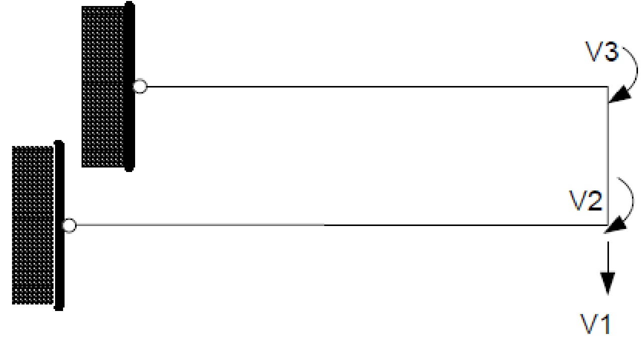

Figure 13: The hinged rigid frame with three deflection directions

By using the force method, the stiffness matrix of the structure in Figure 7.14 can be obtained

$$\begin{bmatrix} k_{11} & k_{12} & k_{13} \\ k_{21} & k_{22} & k_{23} \\ k_{31} & k_{32} & k_{33} \end{bmatrix} \begin{bmatrix} \Delta_1 \\ \Delta_2 \\ \Delta_3 \end{bmatrix} = \begin{bmatrix} F_1 \\ F_2 \\ F_3 \end{bmatrix} \quad (8)$$

where kij is the stiffness coefficient. The definition of a stiffness coefficient is analogous to the definition of the flexibility coefficient: a typical coefficient kij represents the force at i due to a unit displacement applied at . Δi is the deflection in i direction and Fi is the force at i direction. The stiffness coefficient kij can be given by

$$k_{11} = \frac{3EI_2}{L_2^3} + \frac{3EI_1}{L_1^3}$$
$$k_{21} = \frac{3EI_2}{L_2^3}$$
$$k_{31} = \frac{3EI_1}{L_1^3}$$
$$k_{12} = k_{21}$$
$$k_{22} = \frac{3EI_2}{L_2} + \frac{4EI_g}{L_g}$$
$$k_{32} = \frac{3EI_g}{L_g}$$
$$k_{13} = k_{31}$$
$$k_{23} = k_{32}$$
$$k_{33} = \frac{3EI_1}{L_1} + \frac{4EI_g}{L_g}$$

Let F2 and F3 equal to zero, the stiffness coefficient in the direction of V1 can be found from equation 8

$$K_T = k_{11} + \frac{k_{23}k_{31} - k_{33}k_{21}}{k_{22}k_{33} - k_{23}k_{32}} k_{12} + \frac{k_{32}k_{21} - k_{22}k_{31}}{k_{22}k_{33} - k_{23}k_{32}} k_{13}$$

Where K_T is the stiffness coefficient of the hinged frame in the direction of V1.

Figure 14 shows the steps of how to find the final deflection of the U-shape vertical thermal actuator. In Figure 14 (a), the thermal expansion can generate the deflection u at the tip of the actuator, it can be treated as an equivalent force F acting at the tip and generates the same deflection. Hence, the value of force F is uK_T . When the two torsional springs are added to the structure shown in Figure 14 (b), the final deflection of the U-shape vertical thermal actuator can be obtained from

$$u_f = \frac{K_T}{K_T + \frac{K_{b1}}{L_1^2} + \frac{K_{b1}}{L_3^2}} u$$

where K_{b1} and K_{b2} are the torsional spring coefficients of the top and bottom layer short bars, respectively.

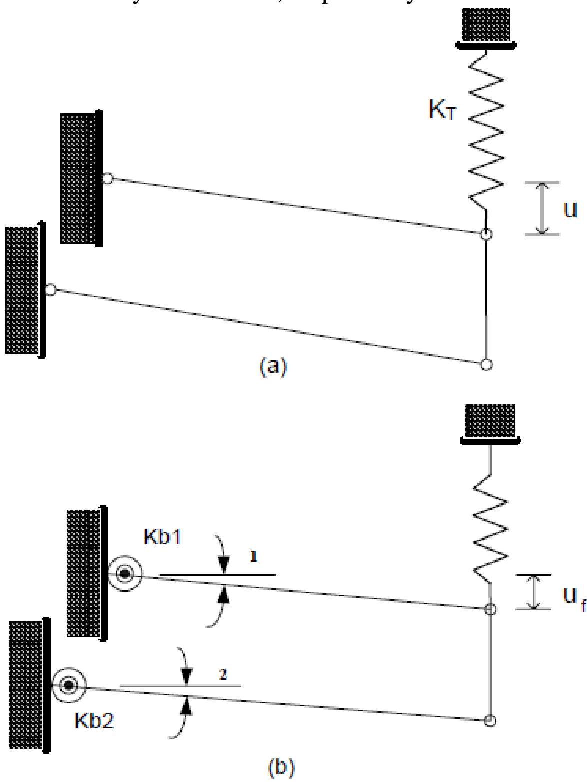

Figure 14: (a) The deflection without torsional springs. (b) The deflection with two torsional springs

E. Simulation results

The deflection as a function of the input voltage is simulated by Coventorware with MemETherm solver. The analytical solution is also provided which is in a good agreement with the simulation results (Figure 15).

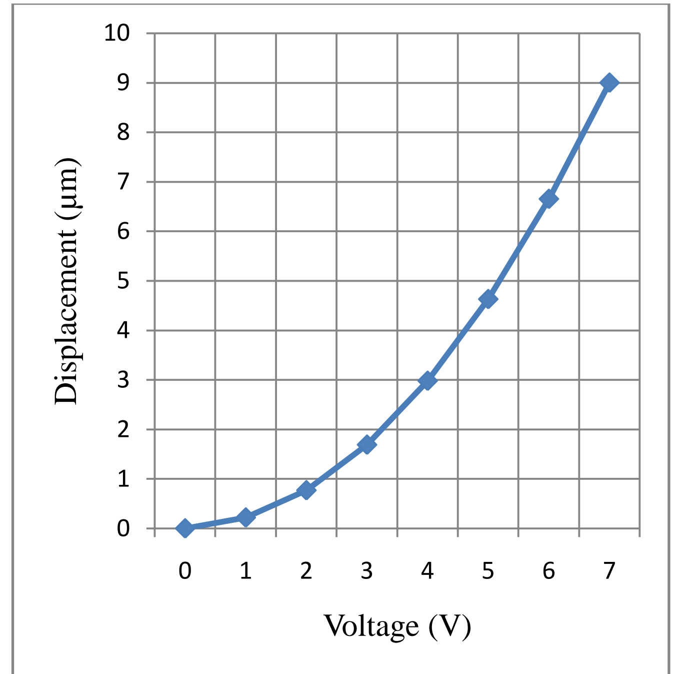

Figure 15: Deflection of the tip of the U-shaped vertical thermal actuatoras a function of input voltage

III VARIABLE CAPACITOR

We present the design and analysis of a MEMS variable capacitor coupled to thermal actuators. The variable capacitor is composed by two main components: 1) the capacitor built by two squared plates, which one plate is mechanically fixed to the substrate and the other is a moving plate having mechanical suspensions (springs) connected from each corner of it to the substrate, and 2) a set of thermal actuators that push the moving plate away from the substrate. The actuators were designed in the previous section. Since we have to move the capacitor plate up and down we choose to employ vertical actuators since it provides us with vertical deflections. Depending on the power applied on the thermal actuators, these would push up the variable plate from its sides, while the suspension pulls the plate down to the substrate for equilibrium. This work includes the design fabrication steps using PolyMUMPS™ process, and provides tables for the resulting values of the variable capacitors. The results accomplished using COVENTORWARE™ software.

A. General Design

The variable capacitor of this work uses two main components: 1) a set of plates composing the capacitor, where one plate is fixed and the other is a moving square plate having mechanical suspension composed of springs connected through the corners of the plate, and 2) a set of electro-thermal actuators that push the variable plate away from the substrate.

The main concept design of the variable capacitors is shown in Figure 16. It is composed of two parallel plates, the lower plate is fixed to the substrate, and the upper plate is the moving plate and it is fixed through a suspension from its corners. Four springs compose the suspension, and these are mechanically fixed to the substrate and they counteract with mechanical force to balance the pushing-up forces applied to the sides of the plate (shown as arrows in Figure16.) The pushing-up forces are applied through the electro-thermal actuators. The balance of the forces, the variable mechanical force produced by the electro-thermal actuators and the counter reacting mechanical force of the springs makes the moving plate steady and so its capacitance with respect to the lower electrostatic plate. Using the PolyMUMPS fabrication process from MEMScAP, we designed this concept idea. Some of the advantages as we have already discussed of using this PolyMUMPS process are:

1) Low cost;

2) It provides three different surface micromachined layers of Polysilicon, two of these layers can be mechanically separated from the base substrate

3) It provides a thin film of gold for electrical interconnect and/or optical reflectivity

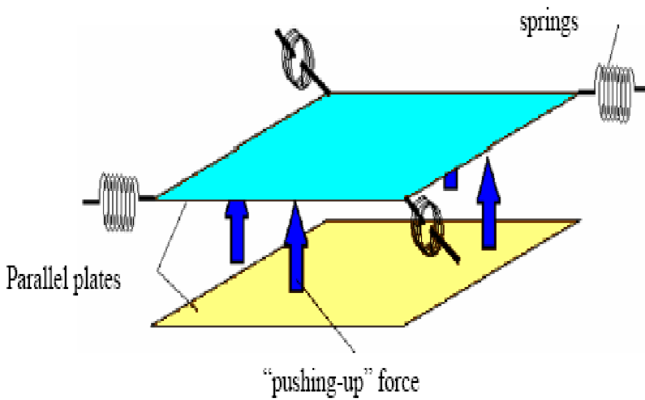

Figure 16: Concept design of the variable capacitor

As we already know the three polysilicon layers of the PolyMUMPS process are electrically conductive. One of these layers is hold to the substrate and is used as an electrical/electrostatic layer (Poly0) and the two others are mechanical layers that can be separated from the substrate (Poly1, and Poly2.It shows four vertical electro-thermal actuators intended to push up the upper plate from its sides; it shows the four springs composing the suspension of the variable capacitor, and the electrical contacts of the upper (variable) and lower (fixed) plates. The following sections provide detailed descriptions of the capacitor's elements.

B. Electro-thermal Mechanical Actuators

We have already discussed the bidirectional vertical actuator. Hear we see that we need to use this vertical actuator to push the capacitor plate upwards, there fore we have to apply voltage to the bottom layer of the actuator; that is made up of poly1, because of which the bottom layer will act as hot arm and the top layer will act as cold arm and moves the vertical actuator upwards. Now the U shap actuator tip has to be connected to the capacitor plate which forms the interfacing section between the vertical actuator and the capacitor.The pushing force by the hot arm in the interfacing section creates a momentum force resulting in a pushing-up force to the end tip of the actuator.

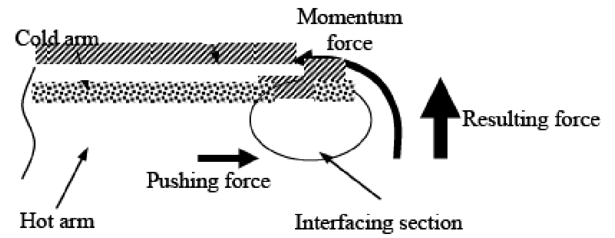

Figure 17. Hot arms pushing the interfacing section showing resulting force

Now we have to find out the resulting force of the actuator. The resulting force of the actuator is found out by inserting a cantilever beam with known dimensions in the interface section of the actuator. The dimensions of the cantilever beam were 2μ width, 1.5μ tall and 150μ length. Running the FEA including cantilever beam, smaller displacement were obtained. Figure 17 shows the 2D model of how the interfacing section is connected to the cantilever beam. Given the displacements of the interface section pushing the beam and using equation 9 and 10 we calculate the resulting forces of the actuators.

$$F = \frac{3EIy(L)}{L^3} \quad (9)$$

$$I = \frac{wt^3}{12} \quad (10)$$

Where, I = Moment of inertia

w = width of cantilever beam

t = thickness/height of the beam

$y(L)$= displacement in the z direction

We have found the spring constant in the previous chapter to be $53\text{N}/\mu\text{m}$ and that by using the above equation we find that the 9 V is the maximum voltage that we can apply to get the deflection for the spring constant found out.

We found out that the spring constant from the previous chapter to be 53N/m.

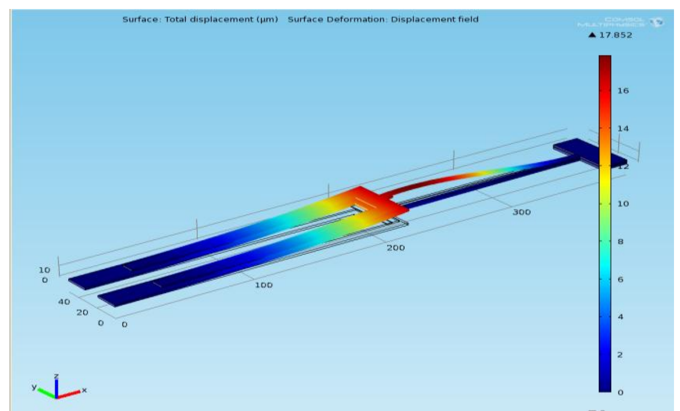

Figure 18:Calculation of force

C. Mechanical Suspensions

We designed suspension systems for the variable capacitors shown in figure 19. The suspensions are fabricated with the electro-mechanical layer Poly2.These suspensions are fixed to the substrate from one side, and hold the capacitor from the other side.
The capacitor plate that we are using is supported by Serpentine flexures. The is as shown in the figure

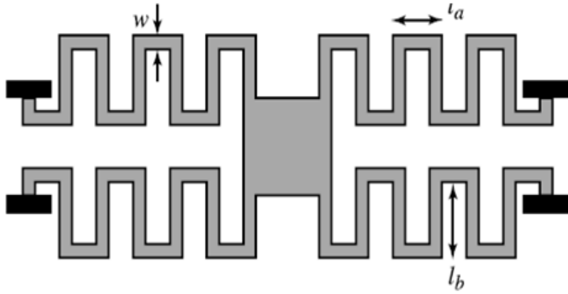

Figure 19:Suspension Spring

In mechanics, and physics, **Hooke's law** of elasticity is an approximation that states that the extension of a spring is in direct proportion with the load applied to it. Many materials obey this law as long as the load does not exceed the material's elastic limit. Materials for which Hooke's law is a useful approximation are known as linear-elastic or "Hookean" materials. Hooke's law in simple terms says that strain is directly proportional to stress.

Mathematically, Hooke's law states that

$$\mathbf{F} = -k\mathbf{x},$$

where

> ***x*** is the displacement of the spring's end from its equilibrium position (a distance, in SI units: meters);
> ***F*** is the restoring force exerted by the spring on that end (in SI units: N or kg·m·s^{-2}); and
> *k* is a constant called the *rate* or *spring constant* (in SI units: N·m^{-1} or kg·s^{-2}).

The spring constant of this serpentine flexures is found out by using the formula [11]:

$$k = \frac{48GJ}{l_a^2\left(\frac{GJ}{EI_X}l_a + l_b\right)n^3} \qquad (11)$$

Where n=number of meanders in the serpentine flexure
$G = \frac{E}{2(1+v)}$ is the torsion modulus
E=Young's modulus
v=poisson's ratio
w=width

$$J = \frac{t^3 w}{3}\left(1 - \left(\frac{192t}{\pi^5 w} * \tanh\left(\frac{\pi w}{2t}\right)\right)\right)$$

$$I_x = \frac{wt^3}{12}$$

The serpentine flexures dimension that are used in our design is given in table 3.

w	1μ
l_a	8μ
l_b	12μ

Table 3: Flexures Parameters.

The spring constant was found to be 0.32N/μm. This shows that the spring is strong and that the actuators fail before the spring would snap off.

D.Variable Capacitor

The design of the variable capacitor is as show in the figure. The 2-D model is shown in the figure 20

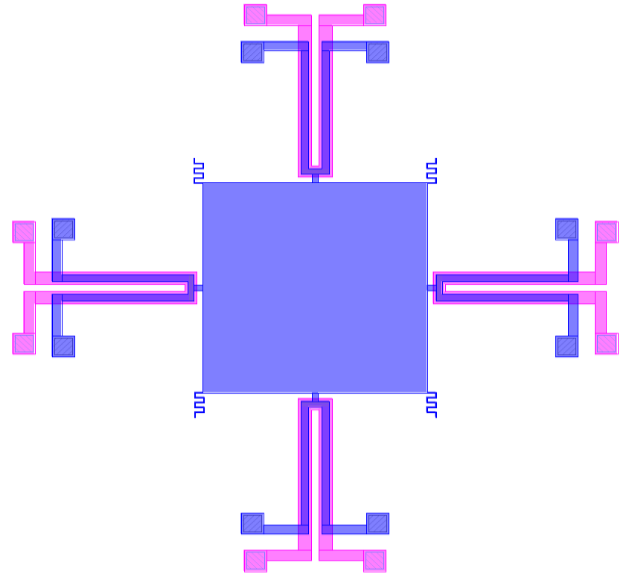

Figure 20: Variable Capacitor

The capacitor is made using PolyMUMPS process. We see that the capacitor plate and the cold arm of the vertical actuator is made up of poly 2 and the hot arm of the vertical actuator is made up of poly 1. Fixed plate below is made up of poly 0.The hot am is anchored by using anchor 1 and the cold arm is anchored using anchor2. The spring is made up of again poly 2 and is fixed to the substrate using anchor 2.

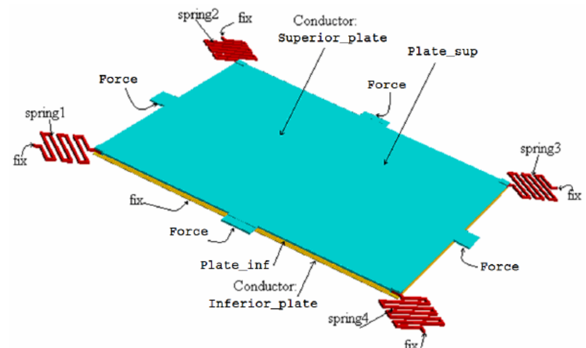

Figure21: Boundary condition

Figure 21 shows the boundary conditions used to simulate and test the suspension systems for different forces applied on the sides of the upper plate. For example, the boundary condition shown as "Force" in figure is used to apply the

pushing-up forces calculated in the thermal actuators' section. Also, the "fix" boundary conditions were used to hold mechanically the suspensions, as well as the lower plate of capacitor. The capacitance is calculated using the following equation

$$C = \frac{\epsilon_0 A}{d}$$

Where A= overlappin plate area
$\epsilon_0 = dielectric\ constant\ of\ air\ (8.854 \times 10^{-14} F/cm)$
d=plate separation

E. Simulation and Results

We see that as we increases the voltage the displacement of the actuators increases which in turn can vary the capacitor. The mimnimum voltage obtained is 0.04 pF and the maximum capacitance that can be obtained is 2.2 pF. Therefore the tuning range of the capacitor is found to be from 0.04 pF to 2.2 pF is shown in table 4.

Voltage	Displacement(μm)	Capacitance(pF)
1	0.38	2.2
2	1.213	0.7
3	2.6	0.3
4	4.54	0.175
5	7.03	0.079
6	10.08	0.079
7	13.69	0.058
8	17.8	0.0447

Table4:Results of variable capacitor

The simulating results is shown in figure 22.This simulating is done using CoventorWare 2010.First the vertical actuator are designed and then we use this vertical actuator to attach it to the capacitor plate.

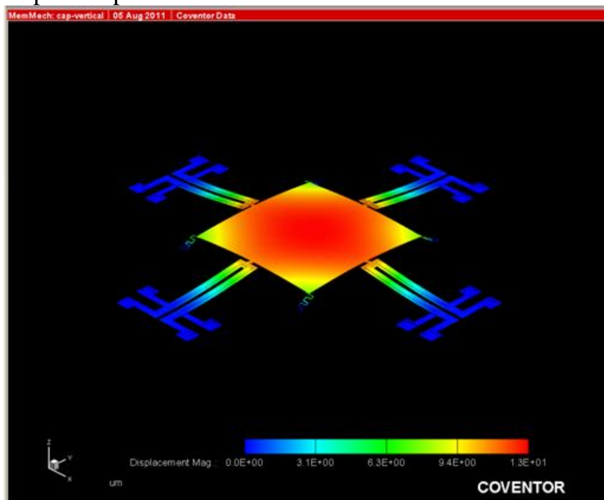

Figure22: Simulation result

CONCLUSION

Based on the strategy of the two-hot-arm horizontal thermal actuator, a U-shape vertical thermal actuator was designed. This novel actuator had the ability to move bidirectionally without any remodification, which indicated twice deflection of the traditional vertical thermal actuators. A new lumped model method was employed to calculate the deflection of the novel bidirectional thermal actuator. Simulation results were provided to show the accuracy of the analytical results.

Using the vertical actuator we further designed the variable capacitor using PolyMUMPS foundry and designed the capacitor tuning range from 2.2 pF to 0.044 pF

Further the actuators designed can be used for many applications such as multi-port switch, micro grippers etc. We can further improve the tunable capacitor design for RF applications.

REFRENCES

[1] Jack W. Judy and Richard S. Muller, "Magnetic microactuation of torsional polysilicon structures," in International Conference on Solid-State Sensors and Actuators Digest of Technical Papers (Transducers '95). 1995.
[2] D. L. Devoe and A. Pisano, "Modeling and optimal design of piezoelectric cantilever microactautors," Journal of Microelectromechanical systems, vol. 6 (3), pp. 266—270, 1997.
[3] Xiaoning Jiang Vijay K. Varadan and Vasundara V. Varadan, Microstereolithography and other fabrication technologies for 3D MEMS, John Wiley and Sons. Ltd, Baffins Lane, Chichester West Sussex,England, 2001.
[4] M. A. Schmidt, "Water-to-wafer bonding for microstructure formation," in Proc. IEEE, 86 (8), pp. 1575—1585. 1998.
[5] M. Madou, Fundamentals of microfabrication, CRC Press, Boca Raton, FLa., 1998.
[6] Gabriel M. Rebeiz "RF MEMS: Theory, Design, and Technology." John Wiley & Sons, 2003, pp 30-31.
[7] Rainee N. Simons "Coplanar Waveguide Circuits, Components, and Systems" A John Wiley and Sons, Inc, Publications, 2001, 387-388

Biography

Suma.N was born in Bangalore,India, on April 10,1986.She graduated from VTU in the year2008 and is currently pursuing Post graduation from VTU.

Pinjare(M’07) was born in Betul Bazar in Betul MadhyaPradesh, India, on May 10, 1953. He graduated from the University of Mysore. He completed his Ph.D from IIT Madras in 1981.He worked at ITI Ltd as Deputy Chief Engineer. Currently he is a professor and PG Coordinator in E&CE Department NMIT Bangalore